Scilight

Regenerative Medicine and Dentistry
https://www.sciltp.com/journals/rmd

Article

Check for updates

A Matrigel-Based Three-Dimensional Culture System for Organoid-Like Differentiation of Human iPS Cell-Derived Embryoid Bodies

Emi Inada [1,*,†], Riko Kuronita [1,†], Issei Saitoh [2], Yasutaka Yanagita [1], Naoko Kubota [1], Yuki Kiyokawa [2], Hirofumi Noguchi [3], Yuria Hori [2], Ryo Bando [2], Masahiko Terajima [4], Yoko Iwase [5], Haruyoshi Yamaza [1] and Masahiro Sato [6]

[1] Department of Pediatric Dentistry, Kagoshima University Graduate School of Medical and Dental Sciences, Kagoshima 890-8544, Japan
[2] Department of Pediatric Dentistry, Division of Oral Structure, Function, and Development, Asahi University School of Dentistry, Gifu 501-0296, Japan
[3] Department of Regenerative Medicine, Graduate School of Medicine, University of the Ryukyus, Okinawa 903-0215, Japan
[4] Department of Oral Anatomy, Asahi University School of Dentistry, Gifu 501-0296, Japan
[5] Department of Dentistry for the Disabled, Asahi University School of Dentistry, Gifu 501-0296, Japan
[6] Department of Genome Medicine, National Center for Child Health and Development, Tokyo 157-8535, Japan
* Correspondence: inada@dent.kagoshima-u.ac.jp
† These authors contributed equally to this work.

How To Cite: Inada, E.; Kuronita, R.; Saitoh, I.; et al. A Matrigel-Based Three-Dimensional Culture System for Organoid-Like Differentiation of Human iPS Cell-Derived Embryoid Bodies. *Regenerative Medicine and Dentistry* **2026**, *3*(3), 13. https://doi.org/10.53941/rmd.2026.100013

Received: 11 July 2026
Revised: 6 August 2026
Accepted: 11 August 2026
Published: 17 August 2026

Abstract: Pluripotent stem cell differentiation is commonly evaluated using in vivo assays; however, these approaches are time-consuming, technically demanding, and limited in experimental controllability. To address these limitations, we aimed to establish a controllable *in vitro* platform for studying the multi-lineage differentiation of human induced pluripotent stem cells (iPSCs) in a three-dimensional (3D) environment. We developed a Matrigel-based 3D culture system for the organoid-like differentiation of human iPSC-derived embryoid bodies (EBs), hereafter referred to as a Matrigel-based *in vitro* 3D differentiation platform (MIVDP). To generate EBs, naïve-like iPSCs carrying enhanced green fluorescent protein (EGFP), introduced via a *piggy*Bac-based transposon system prior to naïve-like conversion, were used. These EBs were then embedded in Matrigel and cultured on membrane filters at the air-liquid interface in a standard medium, such as Dulbecco's modified Eagle's medium (DMEM) supplemented with 10% fetal bovine serum, for up to three weeks. Under these conditions, EBs formed 3D multicellular structures containing various differentiated cell types derived from all three germ layers, as confirmed by histological and immunocytochemical analyses. Furthermore, when cultured in an osteogenic differentiation medium, EB-derived structures preferentially differentiated into osteoblast-like cells, as confirmed by Alizarin Red S staining and osteogenic marker gene expression. Because this system recapitulates certain aspects of multi-lineage differentiation and tissue organization, it can provide a controllable *in vitro* platform for studying the 3D differentiation and lineage specification of human iPSCs.

Keywords: three-dimensional culture system; iPS cells; matrigel; naïve iPSCs; embryoid body; osteogenic differentiation; air-liquid interface (ALI)

1. Introduction

Induced pluripotent stem cells (iPSCs) possess the ability to differentiate into a wide range of cell types and hold significant promise for applications in disease modeling, drug discovery, and regenerative medicine [1–3]. Elucidating the mechanisms underlying their multi-lineage differentiation remains a central challenge for both basic and translational research. There is an increasing interest in developing *in vitro* systems that enable controllable and reproducible analysis of stem cell differentiation within defined conditions [4,5]. In particular, three-dimensional (3D) culture systems have attracted attention because they better recapitulate cell–cell and cell–matrix interactions compared with conventional two-dimensional cultures, thereby facilitating more complex, tissue-like organization [6–9]. Organoid-based approaches have demonstrated the potential of pluripotent stem cells to self-organize into multicellular structures that exhibit aspects of lineage specification and tissue-level organization *in vitro* [10,11].

Embryoid bodies (EBs), commonly formed during iPSCs differentiation, represent an intermediate state containing heterogeneous progenitor populations capable of giving rise to multiple lineages [12,13]. When combined with appropriate extracellular scaffolds, EBs provide a foundation for modeling multi-lineage differentiation in a 3D context [14,15]. Among these scaffolds, Matrigel is widely used because it mimics the extracellular matrix microenvironment and supports the 3D growth and differentiation of various cell types [16,17]. In addition, air-liquid interface (ALI) culture facilitates tissue maturation and 3D organization in various organ culture systems by enhancing nutrient and gas exchange [18].

Based on these considerations, we sought to establish a controllable *in vitro* platform to study the multi-lineage differentiation of human iPSCs in a 3D environment. In the present study, we developed a Matrigel-based 3D culture system where human iPSC-derived EBs are embedded in Matrigel and cultured at an ALI. We designated this system the Matrigel-based *in vitro* 3D differentiation platform (MIVDP).

We hypothesized that EBs cultured within a Matrigel-supported, ALI environment using standard medium [Dulbecco's modified Eagle's medium supplemented with 10% fetal bovine serum (DMEM/10% FBS)] could generate multicellular 3D structures exhibiting multi-lineage differentiation under defined *in vitro* conditions. Using this system, we investigated whether lineage-directed differentiation could be achieved by applying osteogenic induction cues. This study was conducted as a proof-of-concept to demonstrate this hypothesis.

2. Materials and Methods

2.1. Ethics

This study was approved by the Ethics Committee of the Kagoshima University Graduate School of Medical and Dental Sciences (permission no. 220004; dated 14 June 2022).

2.2. Cells

In this study, enhanced green fluorescent protein (EGFP)-expressing mouse B16 melanoma cells [19] and EGFP-expressing human deciduous tooth dental pulp cell (HDDPC)-derived iPSCs [20] were used. The former is a cell line obtained by introducing an EGFP expression vector into mouse B16 melanoma cells and is hereafter referred to as EGFP-B16 cells. As these cells produce melanin pigments, their location can be visibly recognized. The latter are iPSCs obtained by introducing *piggy*Bac-based EGFP expression vectors into HDDPC and subsequently introducing Yamanaka factors (hereinafter referred to as EGFP-iPSCs) [20–22]. After obtaining informed consent, HDPPCs were collected from healthy deciduous teeth extracted due to failure of replacement in our department. Both cell types expressed green fluorescence, enabling easy identification under UV irradiation.

For maintaining EGFP-B16 cells, cultivation was performed in a 60-mm gelatin-coated tissue culture dish (#3010-060; Iwaki Glass Co., Ltd., Tokyo, Japan) with 4 mL of DMEM (#11995040; Thermo Fisher Scientific, Waltham, MA, USA) supplemented with 10% heat-inactivated fetal bovine serum (FBS) (#S1780; Biowest, Nuaillé, France), 50 U/mL penicillin and 50 μg/mL streptomycin (#15140-122; Thermo Fisher Scientific) (which are referred to as DMEM/10% FBS). EGFP-iPSCs were maintained in a 60-mm gelatin-coated tissue culture dish which had been seeded onto mitomycin C (MMC)-treated mouse embryonic fibroblasts (MEFs) with 4 mL of human ES cell culture medium iPSellon (#007001; Cardio, Kobe, Japan) containing 5 ng/mL recombinant human basic fibroblast growth factor (bFGF; #064-04541; Wako Pure Chemical Industries, Ltd., Osaka, Japan).

2.3. 3D Culture System

2.3.1. Experiment 1: 3D Culture of EGFP-B16 Cells

EGFP-B16 cell pellet (5×10^6 cells) was suspended in 60 μL Matrigel [#356255 (Lot: 356255); Corning, NY, USA] in a 1.5-mL tube. The cell suspension was placed on paraffin wax film (#535-02443; Wako Pure Chemical Industries, Ltd.) using a sterile 200 μL-pipette tip and then heated for over 30 min at 37 °C. During this time, the Matrigel solidified into a gel. Conversely, a 35-mm dish (#3000-035; Iwaki Glass Co., Ltd.) was filled with 3 mL of DMEM/10% FBS, onto which an isopore membrane filter (#TSTP01300; Merck Millipore, Darmstadt, Germany) with 3 μm pore size was floated at the ALI. The cell-containing Matrigel was placed at the center of the filter using sterile forceps. Cells were cultured at 37 °C in a 5% CO_2 atmosphere for 20 days. The medium was changed every week. During culture, cell aggregates in Matrigel and EGFP fluorescence were photographed and recorded. Images were selected based on consistent exposure settings, intact Matrigel morphology, and clear EGFP fluorescence; images with air-bubble artifacts, oversaturation, or mechanical distortion were excluded. After 20 days of culture, the dish was filled with 3 mL of 4% paraformaldehyde (PFA) in Dulbecco's modified phosphate-buffered saline without Ca^{2+} and Mg^{2+} (D-PBS(-)) to fix the cell aggregate-containing Matrigel on a filter at 4 °C for 1 week. The fixed tissues were then dehydrated by immersion in 25% sucrose in D-PBS(-) at 4 °C for 2 days, followed by dehydration in 40% sucrose in D-PBS(-) at 4 °C for an additional 4 days. The samples were embedded in optimal cutting temperature (O.C.T.) compounds (Sakura Finetek USA, Inc., St. Torrance, CA, USA), and frozen sections were prepared. Frozen sections were stained with hematoxylin and eosin (H&E).

2.3.2. Experiment 2: 3D Culture of Naïve EGFP-iPSCs

Human iPSCs generally exist in a state called "epiblast stem cells (EpiSCs)", which are slightly more differentiated than mouse iPSCs [3,23]. When differentiation induction is applied to human iPSCs, their differentiation potential has been reported to differ from that of mouse iPSCs under certain conditions. To enhance the differentiation potential of human iPSCs to match that of mouse iPSCs, converting primed human iPSCs to a naïve-like state has been proposed [3,22,24,25]. To convert EGFP-iPSCs to the naïve state, we employed the method described by Hanna et al. [26] with slight modifications [22]. EGFP-iPSCs were cultured in a 60-mm gelatin-coated tissue culture dish that had been seeded with MMC-treated mouse MEFs in 4 mL of medium containing iPSellon, N2 Supplement (#17502-048; Thermo Fisher Scientific), and B27 Supplement (#17504044; Invitrogen, Carlsbad, CA, USA) in a ratio of 96:1:2. In this medium, 5 ng/mL recombinant human bFGF, 0.02 μg/mL recombinant human leukemia inhibitory factor (LIF) (#129-05601; Wako Pure Chemical Industries, Ltd.), 1 μM PD0325901 (#162-25291; Wako Pure Chemical Industries, Ltd.), 10 μM PD98059 (#169-19211; Wako Pure Chemical Industries, Ltd.), 3 μM CHIR99021 (#038-23101; Wako Pure Chemical Industries, Ltd.), 10 μM forskolin (#067-02191; Wako Pure Chemical Industries, Ltd.) and 1 μM kenpaullone (#110-00831; Wako Pure Chemical Industries, Ltd.) were also included. Within 3 to 4 days in culture, human iPSCs form small cell aggregates resembling small moles, a marker of successful conversion to a naïve-like state [22]. The resulting naïve EGFP-iPSCs are hereafter referred to as naïve EGFP-iPSCs. These iPSCs were also converted to a naïve-like state using our previously published protocol, which demonstrated that naïve-like conversion induces expression of naïve-associated markers, including cell-surface SSEA-1 [22]. Consistent with our previous findings, naïve EGFP-iPSCs similarly expressed SSEA-1 following naïve-like conversion, prior to differentiation. Under a stereomicroscope, 5 to 7 moles of naïve EGFP-iPSCs were mechanically aspirated using a 200-μL pipette tip and transferred to the bottom of a 1.5-mL tube. Next, 60 μL Matrigel (chilled at 4 °C) was added to the tube to create a cell suspension. As shown in Experiment 1, the cell suspension in a gel was placed at the center of an isopore membrane filter floating at the ALI on 3 mL of DMEM/10% FBS in a 35-mm dish, and the dish was incubated at 37 °C in a 5% CO_2 atmosphere. The medium was changed every week. During cultivation for up to 20 days, EGFP fluorescence in naïve EGFP-iPSCs in Matrigel was photographed, and the cells were fixed for frozen-section preparation, as described in Experiment 1. Only EGFP-positive areas were analyzed in all downstream imaging, and any faint non-specific signals were excluded by masking/gating to ensure human-cell specificity. Residual MEFs were minimized by manual colony selection prior to 3D culture and excluded from analyses due to a lack of EGFP signal. Some frozen sections were stained with H&E, whereas others were immunostained with antibodies, as described below.

2.3.3. Experiment 3: 3D Culture of EBs Derived from Naïve EGFP-iPSCs

To induce EBs formation from naïve EGFP-iPSCs, small cell aggregates containing more than 50 cells were mechanically detached with a 200-μL pipette tip under a stereomicroscope 3–4 days after naïve-like conversion. These aggregates were then seeded into 3 mL of DMEM/10%FBS in an ultralow attachment 35-mm dish (#MS-9035X; Sumitomo Bakelite Co. Ltd., Tokyo, Japan), and cultured in suspension for 10 days to allow EB formation. Approximately 10 EBs with diameters of less than 1 mm were selected under a stereomicroscope, collected using a 200-μL pipette tip, and transferred to the bottom of a 1.5-mL tube. Next, 60 μL chilled Matrigel (4 °C) was added to suspend the EBs, as described in Experiment 1. The cell suspension in Matrigel was placed onto an isopore membrane filter (3 μm pore size) floating at the ALI of 3 mL of DMEM/10% FBS in a 35-mm dish, and then incubated at 37 °C in a 5% CO_2 atmosphere. The medium was changed every week. After 20 days of culture, the EGFP fluorescence of EB-derived structures in Matrigel was photographed, and the samples were processed for the preparation of frozen sections, as described in Experiment 1. Some frozen sections were stained with H&E, whereas others were immunostained with antibodies, as described below. Residual MEFs were minimized by manual colony selection prior to EB formation and were excluded from analysis due to the absence of EGFP signal. Only intact spherical EBs and well-preserved Matrigel structures were included in analyses; EBs with collapse, fusion, or mechanical disruption were excluded.

2.3.4. Experiment 4: Induction of Differentiation of Naïve EGFP-iPSCs into Osteoblasts

To evaluate whether lineage-directed differentiation could be achieved within the present system, 3D culture of naïve EGFP-iPSC-derived EBs embedded in Matrigel was performed under osteogenic conditions. EBs prepared as described in Experiment 3 were embedded in Matrigel and transferred onto an isopore membrane filter floating at the ALI in a 35-mm dish containing 3 mL of osteogenic differentiation medium (#BMK-R008; Bio Future Technologies, Tokyo, Japan).

The osteogenic differentiation medium contained dexamethasone, L-ascorbic acid 2-phosphate, and glycerol-2-phosphate, which are known to promote osteogenic differentiation of mesenchymal stem cells [27,28]. Cultures were maintained at 37 °C in a 5% CO_2 atmosphere for approximately 20 days to induce bone differentiation. The medium was changed every week.

Following the culture period, EB-derived multicellular structures were processed for frozen section preparation as described in Experiment 1. Osteogenic differentiation was assessed by Alizarin Red S staining (#ARD-A1; PG Research, Tokyo, Japan), which detects calcium deposition associated with mineralization [29]. In addition, immunocytochemical staining was performed for osteocalcin (OCN), a marker of mature osteoblasts.

2.4. Quantification of Differentiated Areas in H&E-Stained Sections

Cryostat sections were stained with H&E. In H&E-stained samples derived from pluripotent cells such as iPSCs, some differentiated cells formed clusters and were clonally expanded [30]. Representative regions exhibiting distinct histological morphologies were enclosed by dotted lines for descriptive morphometric analysis. For the quantitative analysis of H&E-stained samples, the cell area containing differentiated cells was measured using ImageJ (ImageJ bundled with 64-bit Java 8; National Institutes of Health, Bethesda, MD, USA), and the results were represented as a percentage of the cell area containing differentiated cells relative to the total cell area.

To quantify the proportion of differentiated tissue, digital images of H&E-stained sections were analyzed using ImageJ (ImageJ bundled with 64-bit Java 8; National Institutes of Health, Bethesda, MD, USA). Images were acquired under identical microscope and camera settings. For each section, the entire tissue area was manually defined as the region of interest (ROI), while obvious artifacts, tissue tears, folding artifacts, and empty spaces were excluded from analysis. Color deconvolution was performed to separate the hematoxylin and eosin components, and the eosin channel image was used for subsequent analysis. Images were converted to 8-bit grayscale, and a global threshold (Otsu method) was applied under identical conditions to binarize the eosin-positive regions [31]. The positive area within the ROI was measured, and the proportion of differentiated tissue was calculated as the percentage of the eosin-positive area relative to the total tissue area. All images from the iPSC-derived and EB-derived structures were analyzed using identical parameters. Because each condition was represented by a limited number of samples (n = 2 independent experiments), the quantitative analysis serves solely as a descriptive morphometric assessment rather than a basis for statistical comparison. Consequently, no statistical hypothesis testing was performed, and these resulting values should not be interpreted as statistically representative estimates of differentiation efficiency.

2.5. Immunocytochemical Staining

Frozen sections were permeabilized with 0.05% Triton X-100 (#T8787; Sigma-Aldrich, St. Louis, MO, USA) for 3 min at room temperature (approximately 25 °C). After washing with D-PBS(-) containing 1% normal goat serum (NGS) (Invitrogen; hereafter referred to as PBS/NGS), cells were blocked with 20% AquaBlock tm/EIA/WB (#PP82; East Coast Biologics, Inc., North Berwick, ME, USA) for 30 min at 4 °C. After washing with PBS/NGS, the specimens were stained at 4 °C overnight with the following primary antibodies: α-fetoprotein (AFP) (1:200; endodermal marker) (#HPA010607; Atlas Antibodies, Stockholm, Sweden), tubulin beta-3 chain (βIII-tubulin) (1:200; ectodermal marker) (#NB600-936SS; Novus Biologicals, LLC, Centennial, CO, USA), α-smooth muscle actin (α-SMA) (1:200; mesodermal marker) (#NBP1-30894; Novus Biologicals, LLC), SSEA-1 (1:500; #ab16285; Abcam, Cambridge, UK), DDX4/MVH (vasa-homolog) (1:200; marker for germ cells) (#bs-3597R; Bioss Inc., Woburn, MA, USA), and OCN (1:200) (#bs-4917R; Bioss Inc.; marker for osteoblasts).

Notably, SSEA-1 is not a pluripotency marker for conventional human iPSCs. Therefore, rather than serving as an indicator of pluripotency in this study, SSEA-1 was used as an empirical marker to monitor the loss of naïve-like characteristics. This approach was based on our previous findings that the naïve-like conversion of human iPSCs induces SSEA-1 expression, which subsequently decreases upon differentiation [22].

After staining and washing, the specimens were incubated at 4 °C for 2 h with the following secondary antibodies: Alexa Fluor 647-conjugated goat anti-rabbit IgG Fab2 (1:200) (#4414s; Cell Signaling Technology, Tokyo, Japan), and Alexa Fluor 594-conjugated goat anti-mouse IgM (1:200) (#A21044; Invitrogen). After washing with PBS/NGS, nuclei were counterstained using 6-diamidino-2-phenylinodole (DAPI) (#H-1200; Vector Laboratories Inc., Burlingame, CA, USA). The fluorescence was examined using a BX60 fluorescence microscope (Olympus, Tokyo, Japan). Microphotographs were obtained using a Wireless Microscope Camera (J-SCOPE DS-3500WB; SATO SHOUJI Inc., Kanagawa, Japan) controlled by an image measurement function (JCAM; SATO SHOUJI Inc.).

To quantify the proportion of differentiated tissue within each structure, fluorescence images were acquired under identical microscope and exposure settings. Images were included if fluorescence signals were within the dynamic range, free of saturation, and exhibited intact tissue architecture. Images containing folding artifacts, tissue tearing, out-of-focus regions, or a non-specific background exceeding 20% of the total signal were excluded from the analysis. Quantification of differentiation was performed using ImageJ. Regions of interest (ROIs) were defined based on DAPI-positive nuclei and applied to the corresponding fluorescence channels. Background fluorescence was subtracted using a rolling ball radius of 50 pixels. Threshold values were applied uniformly to all images within each staining experiment to binarize the signals. The areas of marker-positive and DAPI-positive regions (white pixels) were measured, and differentiation efficiency was calculated as the percentage of marker-positive area relative to the DAPI-positive area. All images within each experimental group were analyzed using identical parameters. Because this analysis was based on area measurements rather than direct cell counting, the resulting values should be interpreted as relative estimates of marker-positive abundance.

2.6. RT-PCR Analysis

RT-PCR was performed to detect the expression of endogenous pluripotency-associated genes (OCT3/4 and SOX2), an early neural lineage marker (NESTIN) [32,33], and osteogenic lineage-associated markers, including runt-related transcription factor 2 (RUNX2), collagen type I alpha 1 (COL1A1), dentin sialophosphoprotein (DSPP), and OCN. Total RNA was isolated from osteoblasts generated after 3D culture of naïve iPSC-derived EBs in osteoblast differentiation medium (which are defined as "naïve iPSC-EB-OB"), HDDPC (serving as the positive control for OCT3/4, SOX2, NESTIN, RUNX2, COL1A1, DSPP, and OCN [33]), and HDDPC-derived iPSCs (serving as the positive control for OCT3/4 and SOX2 and as the negative control for NESTIN, RUNX2, COL1A1, DSPP, and OCN). cDNA was synthesized from 1 μg of total RNA using the SuperScript™ III First-Strand Synthesis System (#18080051; Thermo Fisher Scientific) with random hexamer primers in a 20 μL reaction volume, following the manufacturer's instructions. Reverse transcription was performed at 50 °C for 50 min, followed by enzyme inactivation at 85 °C for 5 min. A no-template control (designated RT) was included as a negative control for each reaction. Glyceraldehyde-3-phosphate dehydrogenase (GAPDH) was used as the reference gene.

The undiluted cDNA samples (2 μL) were PCR-amplified in a total volume of 20 μL using the AmpliTaq Gold® 360 Master Mix (#4398881; Applied Biosystems, Foster City, CA, USA) with primer sets OCT3/4-S (5′-GGC GGG ACA CCT GGC TTC GGA TTT C-3′; cited from NM_002701.6)/OCT3/4-RV (5′-AGT TCT TTC TGC AGA GCT TTG ATG TC-3′; cited from NM_002701.6) for *OCT3/4*, SOX2-S (5′-GGC AGC TAC AGC ATG ATG CAG GAG C-3′; cited from NM_003106.4)/SOX2-RV (5′-CTG GTC ATG GAG TTG TAC TGC

AGG-3′; cited from NM_003106.4) for *SOX2*, NESTIN-S (5′-CAG CGT TGG AAC AGA GGT TGG-3′; cited from NM_006617.2)/NESTIN-RV (5′-TGG CAC AGG TGT CTC AAG GGT AG-3′; cited from NM_006617.2) for *NESTIN*, RUNX2-S (5′-CCT CAG TGA TTT AGG GCG CA-3′; cited from NM_001369405.1)/RUNX2-RV (5′-TCT GTA ATC TGA CTC TGT CCT TG-3′; cited from NM_001369405.1) for *RUNX2*, COL1A1-S (5′-GGC CAA GAC GAA GAC ATC CCA-3′; cited from NM_000088.4)/ COL1A1-RV (5′-ATC ACG TCA TCG CAC AAC ACC-3′; cited from NM_000088.4) for *COL1A1*, DSPP-S (5′-AAA GTG GTG TCC TGG TGC AT-3′; cited from NM_014208.3)/DSPP-RV (5′-CCT GGA TGC CAT TTG CTG TG-3′; cited from NM_014208.3) for *DSPP*, OCN-S (5′-CCC TTT CTC CTG TCC GGA TG-3′; cited from AY147065.1)/OCN-RV (5′-GCT GAG CTC TAG GGG AGT CT-3′; cited from AY147065.1) for *OCN*, and GAPDH-S (5′-GTC TCC TCT GAC TTC AAC AGC G-3′; cited from NM_002046)/GAPDH-RV (5′-ACC CTG TTG CTG TAG CCA-3′; cited from NM_002046) for *GAPDH*.

PCR cycling conditions were as follows: initial denaturation at 95 °C for 10 min, followed by 36 cycles of denaturation at 95 °C for 30 s, annealing at 52 °C for 30 s, and extension at 72 °C for 30 s, with a final extension at 72 °C for 5 min. RT-PCR in this study was performed as a qualitative assessment to confirm lineage-specific gene expression rather than to quantify transcriptional changes over time. No statistical tests were applied because the results were qualitative and used for lineage confirmation rather than quantitative comparison.

3. Results

3.1. Experiment 1: 3D Culture of EGFP-B16 Cells

To assess whether formation of 3D cellular aggregates could be achieved with this Matrigel-based ALI culture system, EGFP-B16 cells were embedded in Matrigel and cultured in DMEM/10% FBS for 3 weeks (Figure 1A). During the culture period, the cells initially dispersed throughout the scaffold. By day 4, the cells migrated toward the center and continued to proliferate thereafter. As a result, the scaffold was progressively occupied by pigmented cells (Supplementary Figure S1A). Fluorescence observation on day 20 of culture revealed EGFP-derived green fluorescence within the cell aggregates, indicating the presence of viable cells (Supplementary Figure S1A). Histological analysis of frozen sections prepared on day 20 showed a relatively homogeneous distribution of cells within the Matrigel scaffold (Figure 1B(a)). Notably, melanin-containing cells were evident in the 3D structures (arrows in Figure 1B(b–d)). These observations provide proof-of-concept evidence that the Matrigel-based ALI culture system supports the formation and maintenance of 3D cellular aggregates under the described conditions.

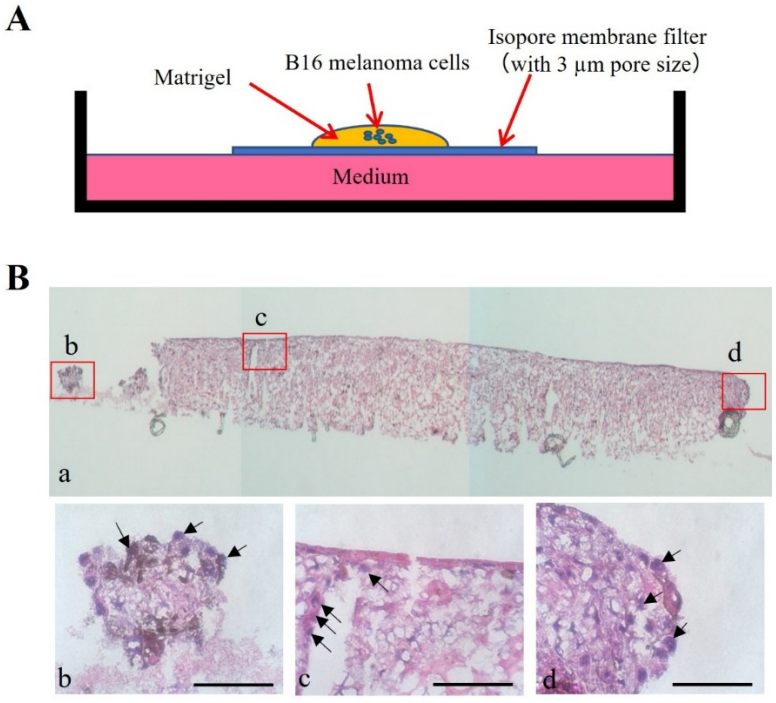

Figure 1. Culture of EGFP-B16 cells in Matrigel-based 3D system up to day 20. (**A**) Schematic representation of the 3D culture system. A Matrigel drop (60 μL) containing an EGFP-B16 cell pellet (5×10^6) was placed on an

isopore membrane filter positioned at the ALI above the culture medium. (**B**) Histological analysis of EGFP-B16 cell aggregates after 20 days of culture. Frozen sections reveal a relatively homogeneous distribution of cells within the Matrigel scaffold in (a). Boxed regions (b–d), including areas with melanin-containing cells (arrows), are shown at a higher magnification in the corresponding panels of (a). Scale bars = 50 μm.

3.2. Experiment 2: 3D Culture of Single Naïve EGFP-iPSCs

To assess whether multi-lineage differentiation could be achieved with this Matrigel-based ALI culture system, single naïve EGFP-iPSCs were embedded in Matrigel and cultured in DMEM/10% FBS for 3 weeks (Figure 2A). During the culture period, the cells proliferated and aggregated toward the center of the scaffold (Supplementary Figure S1B). Fluorescence imaging on day 20 revealed EGFP-derived green fluorescence within the cell aggregates, indicating that the cells remained viable (Supplementary Figure S1B). Histological analysis showed that the resulting structures contained a relatively low proportion of differentiated tissue, with an eosin-positive area of 38.1%. (Figure 2B(a)). A large portion of the structure was composed of loosely organized mesenchyme-like cells with limited evidence of structural organization (Figure 2B(b,h)). There were also small regions exhibiting epithelial-like features (Figure 2B(c,h)), increased intercellular space (Figure 2B(d,h)), an abundance of cells with cuboidal nuclei and eosinophilic cytoplasm (Figure 2B(e,h)), vascular endothelial cells [Figure 2B(f(arrow),h)], or eosin-positive cells [Figure 2B(g(arrow),h)].

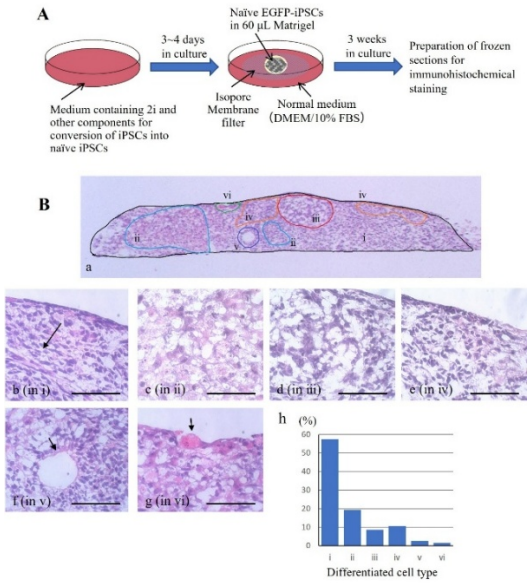

Figure 2. 3D culture of naïve EGFP-iPSCs in a Matrigel-based 3D system up to day 20. (**A**) Schematic representation of the culture system. A Matrigel drop (60 μL) containing naïve EGFP-iPSCs (5 to 7 aggregates) was placed on an isopore membrane filter positioned at the ALI above DMEM/10% FBS. (**B**) Histological analysis of structures derived from naïve EGFP-iPSCs after 20 days of culture. (a) H&E-stained section showing a low degree of cellular differentiation, with regions containing differentiated cells indicated by dotted lines (i–vi). (b–g) Higher magnification views of representative areas indicated in (a), showing various cellular morphologies, including loosely distributed mesenchyme-like cells (arrow in b; magnified from i), regions with epithelial-like features(c; magnified from ii), areas with increased intercellular space (d; magnified from iii), cells enriched with cells with cuboidal nuclei and eosinophilic cytoplasm (e; magnified from iv), vascular endothelial cells (arrow in f; magnified from v) or eosin-positive cells (arrow), which may be components of sebaceous glands, cartilage, or muscle tissue (g; magnified from vi). (h) Descriptive morphometric analysis of representative morphologically differentiated regions (i–vi). The values represent the relative proportion of these regions within the analyzed section and are not intended to indicate absolute differentiation ratios of the entire structure. Scale bars = 50 μm.

Immunocytochemical analyses confirmed the presence of lineage-marker–positive cells, including AFP-positive (endoderm), α-SMA-positive (mesoderm), and βIII-tubulin-positive (ectoderm) cells (Figure 3(a–i)). Quantitative analysis revealed that 29.5% of cells were AFP-positive, 16.9% were α-SMA-positive, and 63.2% were βIII-tubulin-positive. Staining with anti-SSEA-1 showed that 28.1% of the cells remained SSEA-1-positive (Figure 3(j–l)). In this study, SSEA-1 was used to monitor the retention of naïve-like characteristics rather than as a marker of pluripotency. In addition, staining with anti-DDX4/MVH revealed a small population of germ cell–

like cells (3.8%) (Figure 3(m–o)). These results indicate that while structures derived from single naïve iPSCs contained cells expressing markers of all three germ layers, the overall degree of differentiation and structural organization was limited under these conditions.

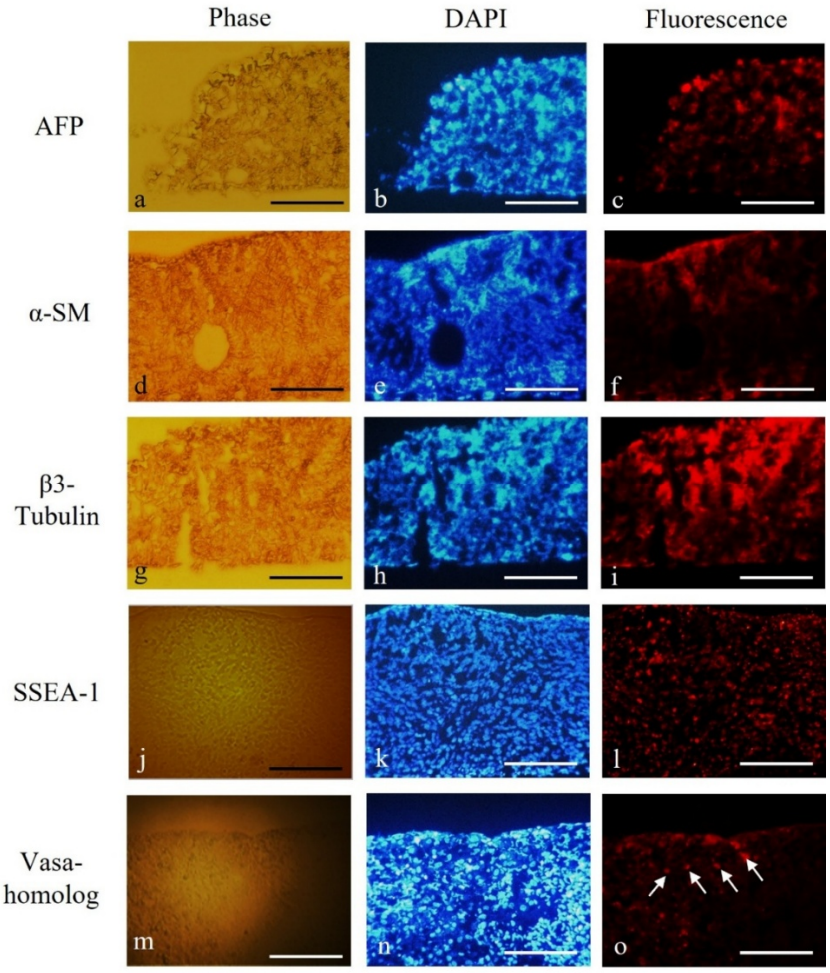

Figure 3. Immunohistochemical analysis of cell aggregates derived from naïve EGFP-iPSCs (shown in Figure 2B) using lineage specific and undifferentiated cell markers.

3.3. Experiment 3: 3D Culture of EBs Derived from Naïve EGFP-iPSCs

To assess whether multi-lineage differentiation could be achieved with the Matrigel-based ALI culture system, EBs derived from naïve EGFP-iPSCs were embedded in Matrigel and cultured in DMEM/10% FBS for 3 weeks (Figure 4A). During the culture period, the EB-derived aggregates increased in size and became concentrated within the Matrigel scaffold (Supplementary Figure S1C). By day 20, these structures had formed a single, cohesive multicellular mass (Supplementary Figure S1C). Fluorescence observation confirmed the presence of EGFP-positive cells, indicating sustained cell viability throughout the culture period (Supplementary Figure S1C). Histological analysis showed that the EB-derived structures exhibited a higher proportion of differentiated tissue compared with those derived from single naïve iPSCs, with an eosin-positive area of 55.1% (Figure 4B). A large portion of the structure consisted of mesenchyme-like cells with wide intercellular spaces and cuboidal nuclei (Figure 4B(b,h)). Smaller regions exhibited epithelial-like structures lining the intestinal lumen [Figure 4B(c(arrow),h)], adipocyte-like cells [Figure 4B(d(arrow),h)], and eosin-rich fibroblastic cells with variable intercellular spacing [Figure 4B(e,h)]. Additionally, we observed structures enriched with eosinophilic immature cells, which are likely smooth muscle precursors [Figure 4B(f,h)], as well as structures resembling lumen-like or tubular patterns [Figure 4B(g,h)].

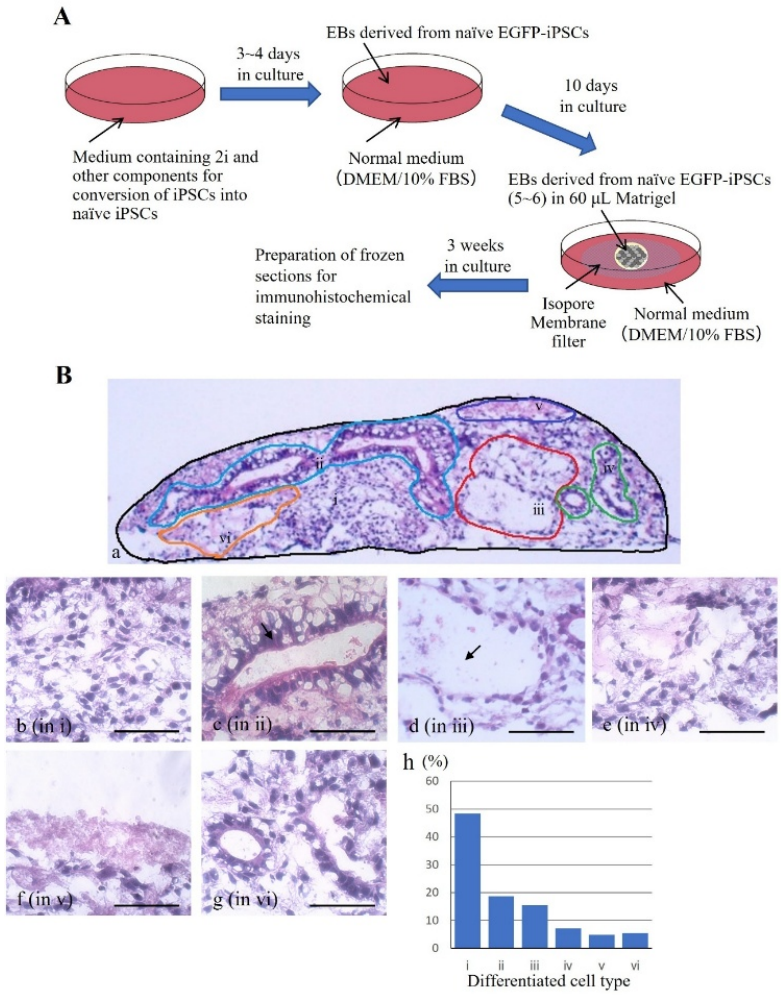

Figure 4. 3D culture of naïve EGFP-iPSC-derived EBs in Matrigel-based 3D system up to day 20. (**A**) Schematic representation of 3D culture system. A 60-µL Matrigel drop containing naïve EGFP-iPSC-derived EBs (approximately 10 EBs, <1 mm diameter) was placed on an isopore membrane filter positioned at the ALI above DMEM/10% FBS. (**B**) Histological analysis of EB-derived structures after 20 days of culture. (a) H&E-stained section showing multicellular structures with higher cellular density and greater morphological complexity compared than those derived from single naïve iPSCs (Figure 2). Dotted lines indicate regions used for quantitative analysis (i–vi). (b–g) Higher magnification views of representative regions indicated in (a), showing a range of cellular morphologies, including mesenchyme-like cells with wide intercellular space (b; magnified from i), epithelial-like structures lining the intestinal lumen (arrow in c; magnified from ii), adipocyte-like cells (arrow in d; magnified from iii), eosin-rich fibroblastic cells with variable intercellular spacing (e; magnified from iv), structures enriched with eosin-rich immature cells, probably precursors for smooth muscle (f; magnified from v), and structure resembling lumen-like or tubular patterns (g; magnified from vi). (h) Descriptive morphometric analysis of representative morphologically differentiated regions (i–vi). The values represent the relative proportion of these regions within the analyzed section and are not intended to indicate absolute differentiation ratios of the entire structure. Scale bars = 50 µm.

Immunocytochemical analysis further demonstrated the presence of cells positive for lineage markers corresponding to the three germ layers (Figure 5a–i). Quantitative analysis revealed that 51.5% of cells were AFP-positive (endoderm), 80.1% were α-SMA-positive (mesoderm), and 71.4% were βIII-tubulin-positive (ectoderm). In contrast to the findings in Experiment 2, only a small fraction of cells remained SSEA-1-positive (12.5%) (Figure 5j–l), suggesting a reduction in naïve-like characteristics. In addition, staining with anti-DDX4/MVH revealed the presence of germ cells (8.7%; arrows in Figure 5m–o). These results indicate that EB-derived structures exhibited increased differentiation and a more developed multicellular architecture compared with those derived from single naïve iPSCs under the same culture conditions.

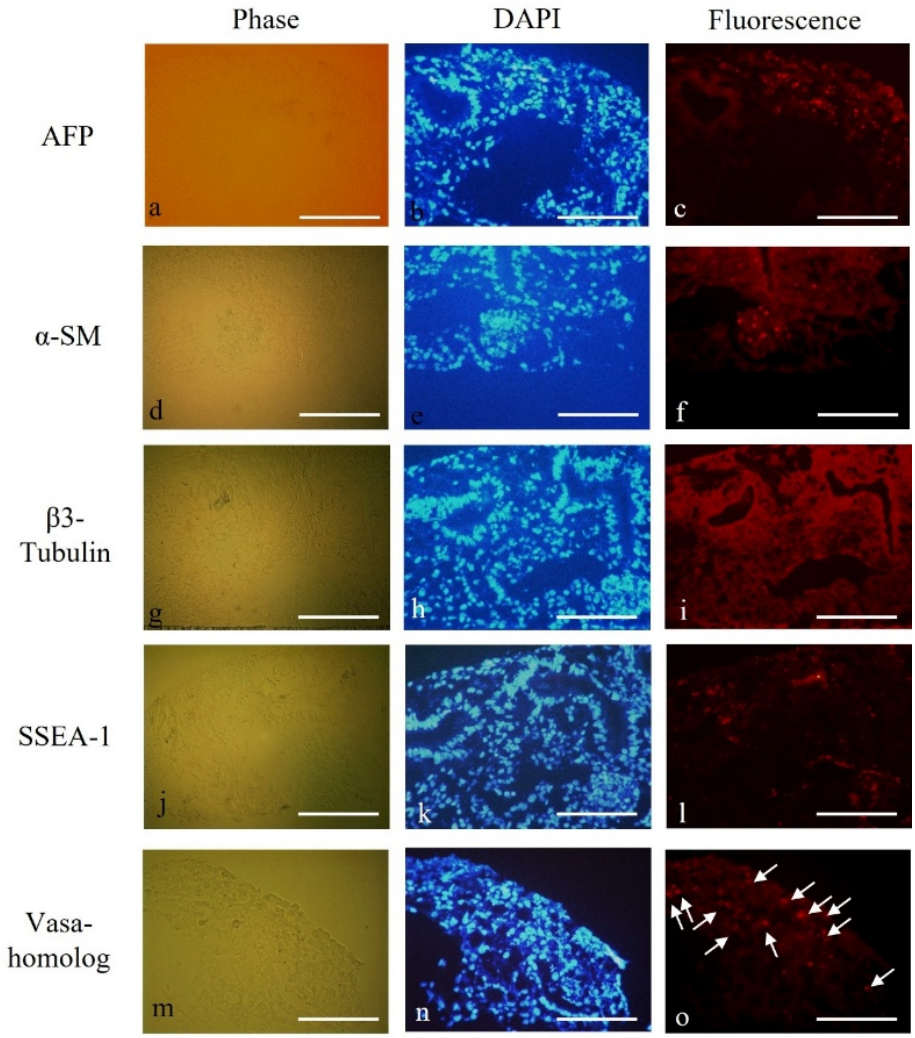

Figure 5. Immunohistochemical analysis of cell aggregates generated from naïve EGFP-iPSC-derived EBs. Frozen sections obtained from day 20 cell aggregates (Figure 4B) were subjected to immunohistochemical staining for lineage-associated and undifferentiated cell markers. Representative images show staining for AFP (endoderm), α-SMA (mesoderm), and βIII-tubulin (ectoderm), indicating the presence of cells expressing markers associated with the three germ layers. Staining for SSEA-1 identifies a smaller population of SSEA-1-positive cells compared with aggregates derived from single naïve EGFP-iPSCs (Figure 3). Staining for DDX4/vasa-homolog (MVH) shows a greater number of positive cells (arrows) compared with Figure 3. EGFP, enhanced green fluorescent protein; iPSCs, induced pluripotent stem cells; EB, embryoid body. Scale bar = 50 μm.

3.4. Experiment 4: Induction of Osteogenic Differentiation from EB-Derived Structures

To assess whether lineage-directed differentiation could be achieved with the Matrigel-based ALI culture system, EB-derived structures embedded in Matrigel were cultured under osteogenic conditions for 3 weeks (Figure 6A). When frozen sections prepared from the resulting cell aggregates were subjected to H&E staining, relatively uniform populations of enlarged differentiated cells were observed, differing markedly from the morphological images obtained in Experiment 3 (Figure 4B vs. Figure 6B(a,b)). These specimens were positive for Alizarin Red S staining, which is frequently used to visualize calcium deposits secreted by osteoblast-like cells during bone formation (Figure 6B(c–e)). Notably, staining was more pronounced around the cells (arrows in Figure 6B(e)), suggesting active mineralization within the extracellular matrix.

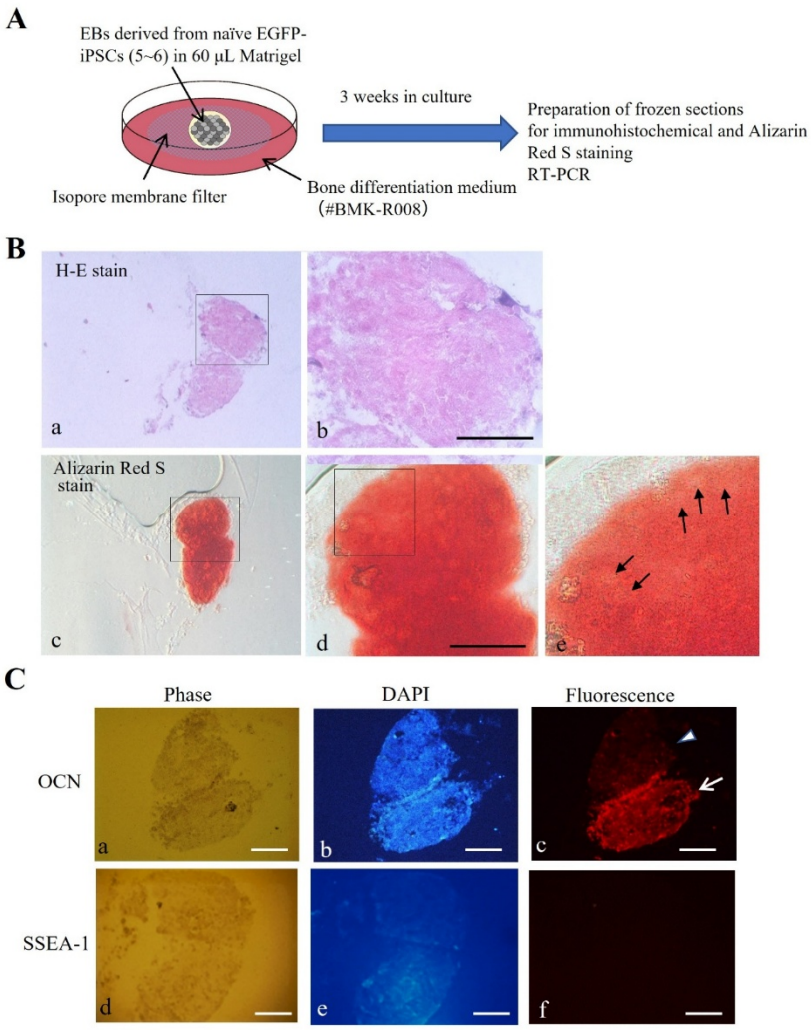

Figure 6. Analysis of osteogenic differentiation in naïve EGFP-iPSC-derived EBs culture. (**A**) Schematic representation of the experimental design. Naïve EGFP-iPSC-derived EBs embedded in Matrigel were cultured in an osteogenic differentiation medium. (**B**) Histological and Alizarin Red S staining of EB-derived aggregates after 20 days of culture under osteogenic conditions. (a, b) H&E staining of the overall structure. (c–e) Alizarin Red S staining showing calcium deposition within the aggregates. Boxed regions in (a) and (c) are shown at higher magnification in (b) and (d), respectively, and the boxed region in (d) is further enlarged in (e). Arrows indicate areas of mineral deposition. (**C**) Immunohistochemical analysis of EB-derived aggregates after osteogenic culture. OCN staining identifies cells expressing OCN, with variable staining intensity across the structure (arrow and arrowhead). SSEA-1-positive cells were rarely detected. EGFP, enhanced green fluorescent protein; iPSCs, induced pluripotent stem cells; EB, embryoid body. Scale bar = 50 µm.

Immunocytochemical analysis further revealed OCN-positive cells within the structures, consistent with osteogenic differentiation (Figure 6C(a–c)). However, some cells exhibited weak OCN staining, while others did not (Figure 6C(c)). These findings indicate that cells positive for Alizarin Red S staining and OCN expression exhibited characteristics consistent with osteoblast-like differentiation. Staining with anti-SSEA-1 was largely absent, suggesting a marked reduction in naïve-like characteristics within these structures (Figure 6C(d–f)).

In addition, RT-PCR analysis demonstrated that osteoblasts derived from the present 3D culture system and positive-control HDDPCs expressed OCT3/4, SOX2, NESTIN, RUNX2, COL1A1, DSPP, and OCN. Although NESTIN is commonly regarded as a neural marker, its expression has also been reported in transient progenitor states during osteogenic differentiation [32–34]; therefore, its detection here likely reflects an intermediate stage rather than lineage deviation. In contrast, HDDPC-derived iPSCs expressed OCT3/4 and SOX2 but not NESTIN, DSPP, OCN, RUNX2 and COL1A1 (Figure 7). Taken together, these findings indicate that EB-derived structures cultured under these conditions exhibit features characteristic of osteogenic differentiation alongside undifferentiated, iPSC-like characteristics. This suggesting that while this system allows for the control of lineage specification through defined culture conditions, this control remains insufficient under the current parameters.

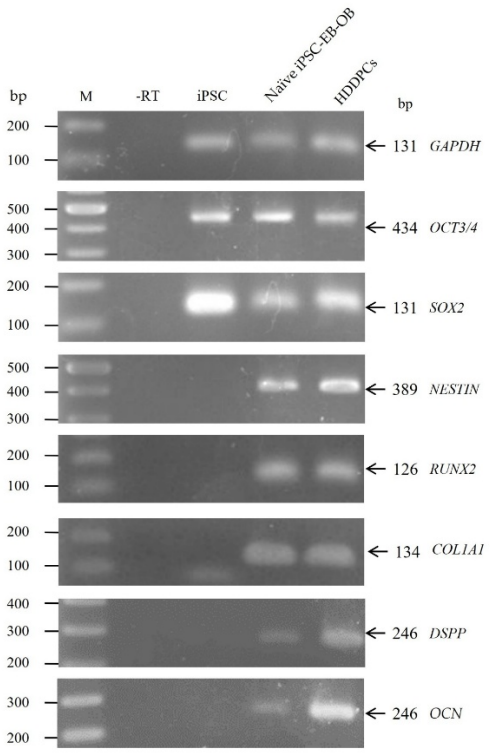

Figure 7. RT-PCR analysis of gene expression in naïve EGFP-iPSC-derived EB cultures under osteogenic conditions (naïve iPSC-EB-OB), compared with HDDPCs and iPSCs. RT-PCR was performed to detect the expression of pluripotency-associated genes (*OCT3/4* and *SOX2*), a neural lineage-associated marker (*NESTIN*), and osteogenic lineage markers (*RUNX2*, *COL1A1*, and *OCN*), together with *DSPP*. Bands corresponding to *OCT3/4* and *SOX2* were detected in iPSCs. In contrast, bands for *NESTIN*, *RUNX2*, *COL1A1*, *DSPP,* and *OCN* were observed in HDDPCs and naïve EGFP-iPSC-derived EB samples cultured under osteogenic conditions. M, 100-bp DNA ladder markers; -RT, no reverse transcriptase control.

4. Discussion

In the present study, we established a Matrigel-based 3D culture system (MIVDP) that enables the formation of multicellular structures comprising all three germ layers via the cultivation of naïve iPSC-derived EBs in a standard medium, such as DMEM/10% FBS, for 3 weeks. These findings align with the established role of EBs as heterogeneous aggregates capable of generating diverse progenitor populations [13,35]. Previous studies have demonstrated that EB formation promotes cell–cell interactions, local signaling gradients, and microenvironmental heterogeneity, thereby facilitating early lineage specification [12]. Although EB-based 3D culture systems do not fully recapitulate in vivo embryogenesis, they are widely accepted as *in vitro* models for studying early differentiation [14,36,37]. In this context, our results extend these findings by showing that EB-derived structures can differentiate within a defined, 3D extracellular matrix-supported environment, such as Matrigel.

Matrigel selection likely contributed substantially to the formation and maintenance of these multicellular structures. It provides a complex mixture of extracellular matrix (ECM) proteins and growth factors that mimic the basement membrane microenvironment, promoting cell adhesion, survival, and differentiation [16,17]. In addition to biochemical signaling, the physical properties of the matrix, including its stiffness and 3D architecture, can drive cellular organization and lineage-specific differentiation [38,39]. Furthermore, the spatial confinement provided by Matrigel embedding could facilitate the establishment of local microenvironments that support heterogeneous differentiation patterns [40–42]. Similar matrix-dependent effects have been reported in various organoid systems, where ECM composition significantly influences tissue architecture and differentiation outcomes [41,43].

In addition to matrix support, ALI culture conditions are likely a crucial component of this system. Widely used in organotypic models, ALI culture and is known to improve oxygenation and nutrient exchange compared to fully submerged conditions [18,44,45]. These properties are particularly important for sustaining thicker or more complex 3D structures, where diffusion limitations can otherwise restrict cell viability and differentiation. In the present system, combination Matrigel embedding with ALI culture likely creates a permissive environment that supports both structural integrity and metabolic activity, thereby contributing to the observed formation of

multicellular 3D structures. This combination may represent a key advantage of the current platform over conventional 3D culture systems.

Another notable finding in this study is the marked difference between structures derived from single naïve iPSCs and those derived from EBs. For instance, whereas the direct culture of naïve iPSCs resulted in relatively poorly differentiated aggregates, EB-derived cultures exhibited substantially increased differentiation and tissue complexity (see Figure 2 vs. Figure 4). This observation supports the concept that EB formation acts as a critical intermediate step that promotes lineage diversification through cellular aggregation and the establishment of heterogeneous microenvironments. Importantly, SSEA-1 was used here as an empirical indicator within this system, rather than as a general marker of pluripotency in human iPSCs. However, the present experimental design does not fully isolate the effects of EB formation from other contributing factors, such as cell density, aggregation state, and culture duration. Therefore, the specific mechanisms underlying these differences require further elucidation.

The ability of the MIVDP to direct differentiation represents another important aspect of its functionality. Under osteogenic culture conditions, EB-derived structures exhibited enhanced mineralization and expression of osteogenic markers, indicating preferential differentiation toward osteoblast-like cells. These findings are consistent with the concept that progenitor populations within EBs retain responsiveness to external cues and can be selectively directed toward specific lineages. This controllability highlights the MIVDP's potential as a platform for studying lineage specification under defined conditions. Conversely, the present EB-derived osteoblast-like cells exhibit osteoblastic properties, as indicated by the expression of osteoblast-specific markers. However, they also show robust expression of OCT3/4 and SOX2 (see Figure 7), suggesting that these cells may retain undifferentiated iPSC-like characteristics and potential tumorigenicity. Therefore, ensuring safety and complete differentiation is essential before applying these cells to future regenerative medicine. To confirm safety (i.e., the absence of tumorigenicity), one approach is to subcutaneously transplant the cells into nude mice to monitor solid tumor formation. To evaluate the completeness of differentiation, further investigation is required to determine whether extending the culture period beyond the current three weeks enhances osteoblastic differentiation. These two aspects will be addressed in future studies.

Unlike conventional organoid protocols designed to generate specific tissue types, the MIVDP supports broad multi-lineage differentiation under experimentally controllable conditions. In this context, this system should be interpreted as an exploratory *in vitro* differentiation platform that yields organoid-like structures, capturing certain aspects of lineage diversification and tissue-level organization. However, several limitations of this study merit acknowledgment. First, the analytical approaches were primarily limited to morphological observations, immunocytochemical analysis, and endpoint RT-PCR. These methods provide limited insight into dynamic gene expression changes and do not fully capture the complexity of lineage specification processes. Second, the limited sample size and the scope of quantitative analysis restrict the statistical robustness of the findings; thus, the resulting values should be interpreted as descriptive indicators of tissue composition rather than definitive measures of differentiation efficiency. Third, the individual contributions of key experimental components—such as Matrigel embedding, ALI culture, and EB formation—were not systematically isolated and evaluated. In addition, because these results are based on a single iPSC line, their generalizability is limited; therefore, further validation across multiple cell lines is warranted.

5. Conclusions

Here, we developed a Matrigel-based *in vitro* culture system, termed MIVDP, which enables the formation of 3D multicellular structures from human iPSC-derived EBs. Under osteogenic conditions, these EB-derived structures exhibited distinct features of lineage-directed differentiation. By allowing controlled investigation of multi-lineage differentiation within a defined environment, this platform offers a complementary *in vitro* approach to elucidate the mechanisms of stem cell differentiation and direct lineage specification. To further enhance the robustness of MIVDP, future studies will focus on inducing differentiation into other cell types (e.g., neurons and adipocytes) using lineage-specific differentiation media.

Supplementary Materials

The additional data and information can be downloaded at: https://media.sciltp.com/articles/others/2608171359197818/RMD-26070114-SI.pdf. Figure S1: Time course observation of cell growth and aggregation within the Matrigel based 3D culture system.

Author Contributions

E.I.: Writing—Original Draft, Writing—review & editing, Conceptualization, Methodology, Validation, Investigation, Resources. R.K.: Writing—review & editing, Investigation. I.S.: Writing—review & editing, Conceptualization, Investigation, Resources. Y.Y.: Writing—review & editing, Investigation. N.K.: Writing—review & editing, Investigation, Resources. Y.K.: Writing—review & editing, Investigation. H.N.: Writing—review & editing, Methodology, Investigation. Y.H.: Writing—review & editing, Investigation. R.B.: Writing—review & editing, Investigation. M.T.: Writing—review & editing, Validation, Investigation. Y.I.: Writing—review & editing, Validation, Investigation. H.Y.: Writing—review & editing, Conceptualization, Investigation. M.S.: Writing—Original Draft, Writing—review & editing, Conceptualization, Methodology, Validation. All authors have read and agreed to the published version of the manuscript.

Funding

This research was funded by the Ministry of Education, Science, Sports, and Culture of Japan (grant numbers 24K13200 to E.I., 23K09441 to N.K., 25K02832 to I.S., and 23K27664 to H.N.).

Institutional Review Board Statement

The study was conducted according to the Ethics Committee of the Kagoshima University Graduate School of Medical and Dental Sciences (permission no. 220004; dated June 14, 2022).

Informed Consent Statement

Informed consent was obtained from all subjects involved in the study.

Data Availability Statement

The original contributions presented in the study are included in the article, and further inquiries can be directed to the corresponding author.

Acknowledgments

We would like to thank Editage (http://www.editage.com, accessed on 11 August 2026) for the English language editing.

Conflicts of Interest

The authors declare no conflict of interest.

Use of AI and AI-Assisted Technologies

No AI tools were utilized for this paper.

References

1. Chehelgerdi, M.; Dehkordi, F.B.; Chehelgerdi, M.; et al. Exploring the promising potential of induced pluripotent stem cells in cancer research and therapy. *Mol. Cancer* **2023**, *22*, 189. https://doi.org/10.1186/s12943-023-01873-0.
2. Liu, G.; David, B.T.; Trawczynski, M.; et al. Advances in Pluripotent Stem Cells: History, Mechanisms, Technologies, and Applications. *Stem Cell Rev. Rep.* **2020**, *16*, 3–32. https://doi.org/10.1007/s12015-019-09935-x.
3. Moradi, S.; Mahdizadeh, H.; Saric, T.; et al. Research and therapy with induced pluripotent stem cells (iPSCs): Social, legal, and ethical considerations. *Stem Cell Res. Ther.* **2019**, *10*, 341. https://doi.org/10.1186/s13287-019-1455-y.
4. Montilla-Rojo, J.; Bialecka, M.; Wever, K.E.; et al. Teratoma Assay for Testing Pluripotency and Malignancy of Stem Cells: Insufficient Reporting and Uptake of Animal-Free Methods-A Systematic Review. *Int. J. Mol. Sci.* **2023**, *24*, 3879. https://doi.org/10.3390/ijms24043879.
5. Smith, L.A.; Hidalgo Aguilar, A.; Owens, D.D.G.; et al. Using Advanced Cell Culture Techniques to Differentiate Pluripotent Stem Cells and Recreate Tissue Structures Representative of Teratoma Xenografts. *Front. Cell Dev. Biol.* **2021**, *9*, 667246. https://doi.org/10.3389/fcell.2021.667246.
6. Antoni, D.; Burckel, H.; Josset, E.; Noel, G., Three-dimensional cell culture: A breakthrough in vivo. *Int. J. Mol. Sci.* **2015**, *16*, 5517–5527.
7. Wu, X.; Su, J.; Wei, J.; Jiang, N.; Ge, X., Recent Advances in Three-Dimensional Stem Cell Culture Systems and Applications. *Stem Cells Int.* **2021**, *2021*, 9477332.

8. Corsini, N.S.; Knoblich, J.A., Human organoids: New strategies and methods for analyzing human development and disease. *Cell* **2022**, *185*, 2756–2769.
9. Novelli, G.; Spitalieri, P.; Murdocca, M.; Centanini, E.; Sangiuolo, F., Organoid factory: The recent role of the human induced pluripotent stem cells (hiPSCs) in precision medicine. *Front. Cell Dev. Biol.* **2022**, *10*, 1059579.
10. Yin, X.; Mead, B.E.; Safaee, H.; et al. Engineering Stem Cell Organoids. *Cell Stem Cell.* **2016**, *18*, 25–38. https://doi.org/10.1016/j.stem.2015.12.005.
11. Artegiani, B.; Hendriks, D. Organoids from pluripotent stem cells and human tissues: When two cultures meet each other. *Dev. Cell.* **2025**, *60*, 493–511. https://doi.org/10.1016/j.devcel.2025.01.005.
12. Zhou, J.; Zhang, Y.; Lin, Q.; et al. Embryoid bodies formation and differentiation from mouse embryonic stem cells in collagen/Matrigel scaffolds. *J. Genet. Genomics* **2010**, *37*, 451–460. https://doi.org/10.1016/S1673-8527(09)60064-3.
13. Guo, N.N.; Liu, L.P.; Zheng, Y.W.; et al. Inducing human induced pluripotent stem cell differentiation through embryoid bodies: A practical and stable approach. *World J. Stem Cells* **2020**, *12*, 25–34. https://doi.org/10.4252/wjsc.v12.i1.25.
14. Zeevaert, K.; Elsafi Mabrouk, M.H.; Wagner, W.; et al. Cell Mechanics in Embryoid Bodies. *Cells* **2020**, *9*, 2270. https://doi.org/10.3390/cells9102270.
15. Goh, S.K.; Olsen, P.; Banerjee, I. Extracellular matrix aggregates from differentiating embryoid bodies as a scaffold to support ESC proliferation and differentiation. *PLoS ONE* **2013**, *8*, e61856. https://doi.org/10.1371/journal.pone.0061856.
16. Benton, G.; Arnaoutova, I.; George, J.; et al. Matrigel: From discovery and ECM mimicry to assays and models for cancer research. *Adv. Drug Deliv. Rev.* **2014,** *79–80*, 3–18. https://doi.org/10.1016/j.addr.2014.06.005.
17. Hughes, C.S.; Postovit, L.M.; Lajoie, G.A. Matrigel: A complex protein mixture required for optimal growth of cell culture. *Proteomics* **2010**, *10*, 1886–1890. https://doi.org/10.1002/pmic.200900758.
18. Homan, K.A.; Gupta, N.; Kroll, K.T.; et al. Flow-enhanced vascularization and maturation of kidney organoids *in vitro*. *Nat. Methods* **2019**, *16*, 255–262. https://doi.org/10.1038/s41592-019-0325-y.
19. Arpino, J.A.; Rizkallah, P.J.; Jones, D.D. Crystal structure of enhanced green fluorescent protein to 1.35 A resolution reveals alternative conformations for Glu222. *PLoS ONE* **2012**, *7*, e47132. https://doi.org/10.1371/journal.pone.0047132.
20. Inada, E.; Saitoh, I.; Kubota, N.; et al. piggyBac Transposon-Based Immortalization of Human Deciduous Tooth Dental Pulp Cells with Multipotency and Non-Tumorigenic Potential. *Int. J. Mol. Sci.* **2019**, *20*, 4904. https://doi.org/10.3390/ijms20194904.
21. Inada, E.; Saitoh, I.; Kubota, N.; et al. Alkaline phosphatase and OCT-3/4 as useful markers for predicting susceptibility of human deciduous teeth-derived dental pulp cells to reprogramming factor-induced iPS cells. *J. Investig. Clin. Dent.* **2017**, *8*, e12236. https://doi.org/10.1111/jicd.12236.
22. Inada, E.; Saitoh, I.; Kubota, N.; et al. Increased Expression of Cell Surface SSEA-1 is Closely Associated with Naive-Like Conversion from Human Deciduous Teeth Dental Pulp Cells-Derived iPS Cells. *Int. J. Mol. Sci.* **2019**, *20*, 1651. https://doi.org/10.3390/ijms20071651.
23. Ebrahimi, M.; Forouzesh, M.; Raoufi, S.; et al. Differentiation of human induced pluripotent stem cells into erythroid cells. *Stem Cell Res. Ther.* **2020**, *11*, 483. https://doi.org/10.1186/s13287-020-01998-9.
24. Kalia, A.K.; Rosseler, C.; Granja-Vazquez, R.; et al. How to differentiate induced pluripotent stem cells into sensory neurons for disease modelling: A functional assessment. *Stem Cell Res. Ther.* **2024**, *15*, 99. https://doi.org/10.1186/s13287-024-03696-2.
25. Balasiddaiah, A.; Moreno, D.; Guembe, L.; et al. Hepatic differentiation of mouse iPS cells and analysis of liver engraftment potential of multistage iPS progeny. *J. Physiol. Biochem.* **2013**, *69*, 835–845. https://doi.org/10.1007/s13105-013-0260-9.
26. Hanna, J.; Cheng, A.W.; Saha, K.; et al. Human embryonic stem cells with biological and epigenetic characteristics similar to those of mouse ESCs. *Proc. Natl. Acad. Sci. USA* **2010**, *107*, 9222–9227. https://doi.org/10.1073/pnas.1004584107.
27. Pittenger, M.F.; Mackay, A.M.; Beck, S.C.; et al. Multilineage potential of adult human mesenchymal stem cells. *Science* **1999**, *284*, 143–147. https://doi.org/10.1126/science.284.5411.143.
28. Mikami, Y.; Omoteyama, K.; Kato, S.; et al. Inductive effects of dexamethasone on the mineralization and the osteoblastic gene expressions in mature osteoblast-like ROS17/2.8 cells. *Biochem. Biophys. Res. Commun.* **2007**, *362*, 368–373. https://doi.org/10.1016/j.bbrc.2007.07.192.
29. Puchtler, H.; Meloan, S.N.; Terry, M.S. On the history and mechanism of alizarin and alizarin red S stains for calcium. *J. Histochem. Cytochem.* **1969**, *17*, 110–124.
30. Sato, M.; Inada, E.; Kubota, N.; et al. Loss of Cell-Cell Contact Inhibits Cellular Differentiation of alpha-Catenin Knock Out P19 Embryonal Carcinoma Cells and Their Colonization into the Developing Mouse Embryos. *BioTech* **2024**, *13*, 41. https://doi.org/10.3390/biotech13040041.
31. Otsu, N. A threshold selection method from gray-level histograms. *IEEE Trans.Syst. Man Cybern.* **1979**, *9*, 62–66. https://doi.org/10.1109/TSMC.1979.4310076.
32. Bernal, A.; Arranz, L. Nestin-expressing progenitor cells: Function, identity and therapeutic implications. *Cell Mol. Life Sci.* **2018**, *75*, 2177–2195. https://doi.org/10.1007/s00018-018-2794-z.
33. Ono, N.; Ono, W.; Mizoguchi, T.; et al. Vasculature-associated cells expressing nestin in developing bones encompass early cells in the osteoblast and endothelial lineage. *Dev. Cell.* **2014**, *29*, 330–339. https://doi.org/10.1016/j.devcel.2014.03.014.

34. Zhu, S.; Chen, W.; Masson, A.; et al. Cell signaling and transcriptional regulation of osteoblast lineage commitment, differentiation, bone formation, and homeostasis. *Cell Discov.* **2024**, *10*, 71. https://doi.org/10.1038/s41421-024-00689-6.
35. Kim, I.S.; Wu, J.; Rahme, G.J.; et al. Parallel Single-Cell RNA-Seq and Genetic Recording Reveals Lineage Decisions in Developing Embryoid Bodies. *Cell Rep.* **2020**, *33*, 108222. https://doi.org/10.1016/j.celrep.2020.108222.
36. Kim, H.; Kim, E. Current Status of Synthetic Mammalian Embryo Models. *Int. J. Mol. Sci.* **2024**, *25*, 12862. https://doi.org/10.3390/ijms252312862.
37. Pettinato, G.; Wen, X.; Zhang, N. Engineering Strategies for the Formation of Embryoid Bodies from Human Pluripotent Stem Cells. *Stem Cells Dev.* **2015**, *24*, 1595–1609. https://doi.org/10.1089/scd.2014.0427.
38. Engler, A.J.; Sen, S.; Sweeney, H.L.; et al. Matrix elasticity directs stem cell lineage specification. *Cell* **2006**, *126*, 677–689. https://doi.org/10.1016/j.cell.2006.06.044.
39. Saraswathibhatla, A.; Indana, D.; Chaudhuri, O. Cell-extracellular matrix mechanotransduction in 3D. *Nat. Rev. Mol. Cell Biol.* **2023**, *24*, 495–516. https://doi.org/10.1038/s41580-023-00583-1.
40. Wang, L.; Chen, A.; Zhang, D.; et al. From Cells to Organoids: Approaches, Regulatory Mechanisms, Applications, and Challenges of Organoids. *Cells* **2025**, *14*, 1898.
41. Sullivan, K.M.; Ko, E.; Kim, E.M.; et al. Extracellular Microenvironmental Control for Organoid Assembly. *Tissue Eng. Part. B Rev.* **2022**, *28*, 1209–1222. https://doi.org/10.1089/ten.TEB.2021.0186.
42. Wolff, L.; Hendrix, S. Rethinking Matrigel: The Complex Journey to Matrix Alternatives in Organoid Culture. *Adv. Sci.* **2025**, *12*, e08734. https://doi.org/10.1002/advs.202508734.
43. Heo, J.H.; Kang, D.; Seo, S.J.; et al. Engineering the Extracellular Matrix for Organoid Culture. *Int. J. Stem Cells* **2022**, *15*, 60–69. https://doi.org/10.15283/ijsc21190.
44. Nossol, C.; Diesing, A.K.; Walk, N.; et al. Air-liquid interface cultures enhance the oxygen supply and trigger the structural and functional differentiation of intestinal porcine epithelial cells (IPEC). *Histochem. Cell Biol.* **2011**, *136*, 103–115. https://doi.org/10.1007/s00418-011-0826-y.
45. Sekiya, S.; Kikuchi, T.; Shimizu, T. Perfusion culture maintained with an air-liquid interface to stimulate epithelial cell organization in renal organoids *in vitro*. *BMC Biomed. Eng.* **2019**, *1*, 15. https://doi.org/10.1186/s42490-019-0017-9.